IEEE Access
Multidisciplinary : Rapid Review : Open Access Journal

Received September 22, 2020, accepted October 3, 2020, date of publication October 13, 2020, date of current version November 13, 2020.

Digital Object Identifier 10.1109/ACCESS.2020.3030648

Virtual Frequency Construction-Based Vector Current Control for Grid-Tied Inverter Under Imbalanced Voltage

WU BINBING[1], TIAN YIZHI[1], CHEN YUXI[2], XIWANG ABUDUWAYITI[1], AND LIANSONG XIONG[3], (Member, IEEE)

[1]School of Electrical Engineering, Xinjiang University, Urumqi 830049, China
[2]Faculty of Engineering, The University of Sheffield, Sheffield S10 2TN, U.K.
[3]School of Automation, Nanjing Institute of Technology, Nanjing 211167, China

Corresponding author: Tian Yizhi (156794979@qq.com)

This work was supported in part by the National Natural Science Foundation of China Fund under Grant 51367017, and in part by the Scientific Research Project for University, Xinjiang Uyghur Autonomous Region, under Grant XJUEDU2017S011.

ABSTRACT This paper proposes a fast phase capture (FPC) scheme and applies it to the control strategy of grid-tied inverters under imbalanced voltage. Firstly, a method for quickly extracting sequence components of power signals is derived through the symmetrical component method, and a real-time phase calculation method is proposed based on the rotating reference frame, thus avoiding the phase-locked loop (PLL) closed-loop adjustment process. Secondly, the grid-tied inverter suppresses the negative sequence current or power fluctuations through the direct resonance controller, so there is no need to separate the dynamically changing sequence current components. Finally, the experimental comparison with the PLL control strategy is carried out based on the RT-LAB platform. Compared with the previous phase-locking scheme, the FPC scheme has a faster phase-locking speed. Therefore, the fault ride-through capability of the grid-tied inverter is improved.

INDEX TERMS Current control, grid-tied inverter, imbalanced grid, phase detection.

I. INTRODUCTION

Three-phase voltage imbalance is a common power system operating conditions, which will seriously interfere with the grid-tied inverter output power quality. For reaching the increasingly demanding application requirements, ensuring the dynamic performance and stable operation of the grid-tied inverter is a prerequisite [1], [2].

Three-phase load overload or imbalance, the short circuit between phases of the line, and single-phase grounding may cause large fluctuations in the voltage of the grid-connected port so that the phase-locked loop (PLL) will produce varying degrees of transient response, which makes the inverter cannot achieve the expected control performance. The speed of PLL's phase detection is one of the main factors that affect inverter control performance. The single synchronous reference frame (SRF-PLL) [3], in the existing PLL scheme, has been widely used in inverter control strategies due to its simple structure and good reliability. However, in the voltage imbalanced state, the voltage sequence component will produce double the fundamental frequency component in the SRF, which makes the PLL unable to accurately phase lock [4]. In order to solve this problem, [5], [6] implement a second-order generalized integrator (SOGI) to phase-shift the grid voltage to obtain the positive sequence component in the stationary reference frame, thereby avoiding the influence of the double frequency component. In [7], a delay operation period filter is developed in dq frame, but in some demanding applications, it is obviously difficult to meet the demand in response time through filter design. In [8], An improved PLL scheme is proposed to enhance the robustness of the power grid in the case of weak power grids. To better solve the phase lock error when the three-phase grid voltage is asymmetry. In [9], an improved soft PLL algorithm that is easy to digitally implement is proposed. According to the symmetry principle of the trigonometric function, an improved strategy eliminates the influence of the double frequency component through the delay link [10]. However, this scheme requires

The associate editor coordinating the review of this manuscript and approving it for publication was Pinjia Zhang.

at least 0.25 power frequency cycles. The above mentioned improved PLL schemes all strive to achieve a better compromise in terms of filtering performance and response time by designing better filters and controller parameters. The phase-locking speed of the PLL is one of the main factors affecting the transient response capability of the inverter. Therefore, a faster phase-locking speed is required in inverter control.

The control methods for grid-tied inverters include hysteretic current control [11], vector current control [12], and direct power control [13]. The hysteresis width of the hysteresis control is difficult to set, and it is hard to achieve in practical use. The vector current control uses the proportional-integral (PI) regulator to control the related current indirectly to achieve the power transmission of the inverter [14], but the PI regulator cannot achieve the control of the ac quantity. In [15], a resonance controller scheme is presented. This method can directly control the ac quantity and realizes its no static error control. In [16], the dual SRF is implemented to control the power transmission of the inverter, but this solution requires a filter to extract the negative sequence component, which increases the complexity of the control system. The above inverter control methods all require the PLL to close-loop adjustment, especially when the grid voltage is imbalanced, the PLL needs to track the grid voltage again, which will affect the transient response capability of the inverter. In [17], based on the instantaneous power theory, a control method without PLL for single-phase converters is employed. Based on direct power control, [18] proposed a control scheme of second-order vector integrator in the SRF without PLL. However, [17], [18] cannot be directly applied to the grid voltage imbalance, and the line current will produce a more serious negative sequence current and power fluctuation. In [19], to eliminate the potential impact of the coupling between the PLL and the grid point of common coupling. A direct power control without PLL scheme is proposed under the imbalanced voltage. However, in practical applications, inverter current control is more universal. In [17]–[19], the less-PLL scheme is improved on the control loop topology to ensure the stable operation of the inverter under the harsh working conditions. However, the dynamic and static response capabilities of the inverter are not considered. Since these less-PLL solutions do not capture the grid voltage phase, the inverter cannot achieve decoupling control, which increases the operating burden of the DSP. The main factors affecting the transient response capability of the inverter are the digital delay process, the control parameter design of the current loop, and the phase lock speed of the PLL. Reference [20] optimizes the current loop parameters through a multi-objective function to improve the transient response capability of the inverter, a simple small signal supplementary control is proposed.

To further shorten the time that the grid-tied inverter bears malfunction, this paper proposes a fast phase capture (FPC) scheme for inverter systems. A sequence component extraction scheme is proposed and the inverter control system does not need to design a filter to eliminate the double frequency component, which improves the sequence component extraction speed and simplifies the system structure. The grid voltage phase is obtained by real-time mathematical calculation, without the need to design an improved PLL. Furthermore, a direct resonance controller is employed to ensure current balance or active power stability. This method does not need to separate the positive and negative sequence components of the line current. This strategy avoids the problems of PLL closed-loop adjustment and parameter design difficulties, so that the negative sequence current compensation and power response ability of the inverter can be improved. FPC scheme can also be extended to the application of harmonic control of active power filters (APF), just by adding the corresponding harmonic elimination algorithm.

The remainder of this paper is organized as follows. Section II analyses the detailed process of sequence component separation. Then, a FPC method for inverter control is proposed to improve the fault ride-through capability in the Section III. The correctness of the proposed method is verified in Section IV. The conclusions are drawn in Section V.

II. SEQUENCE COMPONENT EXTRACTION SCHEME UNDER IMBALANCED VOLTAGE

A. METHOD OF SEQUENCE COPMPONENT CONSTRUCTION

The grid-side voltage is composed of positive sequence and negative sequence components, and its zero sequence component is ignored [19].

$$\boldsymbol{E} = \begin{bmatrix} e_{\mathrm{a}}(t) \\ e_{\mathrm{b}}(t) \\ e_{\mathrm{c}}(t) \end{bmatrix} = \begin{bmatrix} e_{\mathrm{a}}^{+}(t) + e_{\mathrm{a}}^{-}(t) \\ e_{\mathrm{b}}^{+}(t) + e_{\mathrm{b}}^{-}(t) \\ e_{\mathrm{b}}^{+}(t) + e_{\mathrm{c}}^{-}(t) \end{bmatrix} = \begin{bmatrix} E_{\mathrm{m}} \sin(\omega t + \varphi_{\mathrm{a}}) \\ E_{\mathrm{m}} \sin(\omega t + \varphi_{\mathrm{b}}) \\ E_{\mathrm{m}} \sin(\omega t + \varphi_{\mathrm{c}}) \end{bmatrix} \tag{1}$$

$$\boldsymbol{E}^{+} = \begin{bmatrix} e_{\mathrm{a}}^{+}(t) \\ e_{\mathrm{b}}^{+}(t) \\ e_{\mathrm{c}}^{+}(t) \end{bmatrix} = \begin{bmatrix} E_{\mathrm{m}}^{+} \sin(\omega t + \varphi) \\ E_{\mathrm{m}}^{+} \sin(\omega t - 2\pi/3 + \varphi) \\ E_{\mathrm{m}}^{+} \sin(\omega t + 2\pi/3 + \varphi) \end{bmatrix} \tag{2}$$

$$\boldsymbol{E}^{-} = \begin{bmatrix} e_{\mathrm{a}}^{-}(t) \\ e_{\mathrm{b}}^{-}(t) \\ e_{\mathrm{c}}^{-}(t) \end{bmatrix} = \begin{bmatrix} E_{\mathrm{m}}^{-} \sin(\omega t + \delta) \\ E_{\mathrm{m}}^{-} \sin(\omega t + 2\pi/3 + \delta) \\ E_{\mathrm{m}}^{-} \sin(\omega t - 2\pi/3 + \delta) \end{bmatrix} \tag{3}$$

where ω refers to the actual angular frequency of the grid, the superscripts $+$, $-$ refer to the positive and negative sequence components, E_{m}, φ_{s} refer to the amplitude and initial phase of the grid voltage, $E_{\mathrm{m}}^{\mathrm{s}}$, φ, and δ refer to the sequence component amplitude and initial phase, respectively.

Based on abc/dq coordinate transformation matrix, (1) can be rewritten as

$$\begin{bmatrix} E_d \\ E_q \end{bmatrix} = \boldsymbol{T}_{\mathrm{abc/dq}}(\omega t) \begin{bmatrix} e_{\mathrm{a}}(t) \\ e_{\mathrm{b}}(t) \\ e_{\mathrm{c}}(t) \end{bmatrix} \tag{4}$$

where

$$\boldsymbol{T}_{\mathrm{abc/dq}}(\omega t) = \frac{2}{3}\begin{bmatrix} \sin\omega t & \sin\left(\omega t - 2\pi/3\right) & \sin\left(\omega t + 2\pi/3\right) \\ \cos\omega t & \cos\left(\omega t - 2\pi/3\right) & \cos\left(\omega t + 2\pi/3\right) \end{bmatrix}$$

According to (4), grid-side voltage can be expressed as

$$\begin{cases} E_d = E_{\mathrm{m}}^{+}\cos\varphi - E_{\mathrm{m}}^{-}\cos\left(2\omega t + \delta\right) \\ E_q = E_{\mathrm{m}}^{+}\sin\varphi + E_{\mathrm{m}}^{-}\sin\left(2\omega t + \delta\right) \end{cases} \tag{5}$$

It can be seen from (5) that the grid-side voltage in the SRF contains a double frequency component. In the past solutions, to accurately lock the phase and achieve the control goal of the inverter, a corresponding filter should be designed to eliminate doble frequency components. Without considering the phase-locking process, the fastest sequence component extraction scheme takes at least 5ms (when the grid frequency is 50Hz) [7]. Therefore, the phase-locking process under the imbalanced voltage restricts the transient response capability of the inverter.

The FPC scheme is shown in Figure 1. The three-phase voltage $\boldsymbol{E}$ is regarded as three independent single-phase voltages $e_{\mathrm{a}}(t)$, $e_{\mathrm{b}}(t)$, $e_{\mathrm{c}}(t)$ (as shown in Part 1). Construct three fictive orthogonal variables of single-phase voltage, and combine the three groups of orthogonal variables in pairs to obtain the phasor form of each phase voltage (including amplitude and phase information). Apply the sequence component transformation matrix to solve the positive sequence component and negative sequence component in the form of voltage phasor (as shown in Part 2). Finally, the α-axis component is obtained through the inverse calculation of the voltage phasor to obtain the positive and negative sequence components of the voltage (as shown in Part 3). Among them, part 2 can be simplified into part 4 through mathematical calculations. The specific derivation process is as follows

$$\dot{\boldsymbol{E}}_F^{\mathrm{s}} = \dot{\boldsymbol{T}}^{\mathrm{s}}\dot{\boldsymbol{E}}_F \tag{6}$$

where $\dot{\boldsymbol{E}}_F$ is the fictive grid voltage, $\dot{\boldsymbol{E}}_F^{\mathrm{s}}$ and $\dot{\boldsymbol{T}}^{\mathrm{s}}$ are the sequence component of the fictive grid voltage and transformation matrix of the sequence component, respectively.

$$\dot{\boldsymbol{T}}^{+} = \frac{1}{3}\begin{bmatrix} 1 & a & a^2 \\ a^2 & 1 & a \\ a & a^2 & 1 \end{bmatrix} \quad \dot{\boldsymbol{T}}^{-} = \frac{1}{3}\begin{bmatrix} 1 & a^2 & a \\ a^2 & a & 1 \\ a & 1 & a^2 \end{bmatrix}$$

$$a = \mathrm{e}^{\mathrm{j}2\pi/3}$$

$\dot{\boldsymbol{E}}_F, \dot{\boldsymbol{E}}_F^{\mathrm{s}}$ can be expressed in the $\alpha\beta$-frame as

$$\dot{\boldsymbol{E}}_F = \boldsymbol{E}_\alpha + \mathrm{j}\boldsymbol{E}_\beta \tag{7}$$

$$\dot{\boldsymbol{E}}_F^{\mathrm{s}} = \boldsymbol{E}_\alpha^{\mathrm{s}} + \mathrm{j}\boldsymbol{E}_\beta^{\mathrm{s}} \tag{8}$$

where

$$\begin{aligned} \boldsymbol{E}_\alpha &= \begin{bmatrix} e_{\mathrm{a}\alpha}(t) & e_{\mathrm{b}\alpha}(t) & e_{\mathrm{c}\alpha}(t) \end{bmatrix}^{\mathrm{T}} \\ \boldsymbol{E}_\beta &= \begin{bmatrix} e_{\mathrm{a}\beta}(t) & e_{\mathrm{b}\beta}(t) & e_{\mathrm{c}\beta}(t) \end{bmatrix}^{\mathrm{T}}, \\ \boldsymbol{E}_\alpha^{\mathrm{s}} &= \begin{bmatrix} e_{\mathrm{a}\alpha}^{\mathrm{s}}(t) & e_{\mathrm{b}\alpha}^{\mathrm{s}}(t) & e_{\mathrm{c}\alpha}^{\mathrm{s}}(t) \end{bmatrix}^{\mathrm{T}} \\ \boldsymbol{E}_\beta^{\mathrm{s}} &= \begin{bmatrix} e_{\mathrm{a}\beta}^{\mathrm{s}}(t) & e_{\mathrm{b}\beta}^{\mathrm{s}}(t) & e_{\mathrm{c}\beta}^{\mathrm{s}}(t) \end{bmatrix}^{\mathrm{T}}. \end{aligned}$$

In the sequence component structure, the actually measured three-phase grid voltage is taken as the α-axis component, and its corresponding fictive orthogonal variable is taken as the β-axis component.

$$\boldsymbol{E}_\alpha = \boldsymbol{E}\ \boldsymbol{E}_\alpha^{+} = \boldsymbol{E}^{+}\ \boldsymbol{E}_\alpha^{-} = \boldsymbol{E}^{-} \tag{9}$$

$$\boldsymbol{E}_\beta = \boldsymbol{E}_\perp = \begin{bmatrix} e_{\mathrm{a}\perp}(t) \\ e_{\mathrm{b}\perp}(t) \\ e_{\mathrm{c}\perp}(t) \end{bmatrix} = \begin{bmatrix} E_{\mathrm{m}}\cos\left(\omega t + \varphi_{\mathrm{a}}\right) \\ E_{\mathrm{m}}\cos\left(\omega t + \varphi_{\mathrm{b}}\right) \\ E_{\mathrm{m}}\cos\left(\omega t + \varphi_{\mathrm{c}}\right) \end{bmatrix} \tag{10}$$

$$\boldsymbol{E}_\beta^{+} = \boldsymbol{E}_\perp^{+} = \begin{bmatrix} e_{\mathrm{a}\perp}^{+}(t) \\ e_{\mathrm{b}\perp}^{+}(t) \\ e_{\mathrm{c}\perp}^{+}(t) \end{bmatrix} = \begin{bmatrix} E_{\mathrm{m}}^{+}\cos\left(\omega t + \varphi\right) \\ E_{\mathrm{m}}^{+}\cos\left(\omega t - 2\pi/3 + \varphi\right) \\ E_{\mathrm{m}}^{+}\cos\left(\omega t + 2\pi/3 + \varphi\right) \end{bmatrix} \tag{11}$$

$$\boldsymbol{E}_\beta^{-} = \boldsymbol{E}_\perp^{-} = \begin{bmatrix} e_{\mathrm{a}\perp}^{-}(t) \\ e_{\mathrm{b}\perp}^{-}(t) \\ e_{\mathrm{c}\perp}^{-}(t) \end{bmatrix} = \begin{bmatrix} E_{\mathrm{m}}^{-}\cos\left(\omega t + \delta\right) \\ E_{\mathrm{m}}^{-}\cos\left(\omega t + 2\pi/3 + \delta\right) \\ E_{\mathrm{m}}^{-}\cos\left(\omega t - 2\pi/3 + \delta\right) \end{bmatrix} \tag{12}$$

According to (9) ~ (12), (7) and (8) can be rewritten as

$$\dot{\boldsymbol{E}}_F = \boldsymbol{E} + \mathrm{j}\boldsymbol{E}_\perp \tag{13}$$

$$\dot{\boldsymbol{E}}_F^{\mathrm{s}} = \boldsymbol{E}^{\mathrm{s}} + \mathrm{j}\boldsymbol{E}_\perp^{\mathrm{s}} \tag{14}$$

Substituting (13) and (14) into (6) and taking the real part, the sequence component expression of the grid voltage can be deduced as

$$\begin{cases} \boldsymbol{E}^{+} = T_\alpha^{+}\boldsymbol{E} + T_\beta^{+}\boldsymbol{E}_\perp \\ \boldsymbol{E}^{-} = T_\alpha^{-}\boldsymbol{E} + T_\beta^{-}\boldsymbol{E}_\perp \end{cases} \tag{15}$$

where

$$T_\alpha^{+} = \frac{1}{6}\begin{bmatrix} 2 & -1 & -1 \\ -1 & 2 & -1 \\ -1 & -1 & 2 \end{bmatrix} \quad T_\beta^{+} = \frac{\sqrt{3}}{6}\begin{bmatrix} 0 & 1 & -1 \\ -1 & 0 & 1 \\ 1 & -1 & 0 \end{bmatrix}$$

$$T_\alpha^{-} = \frac{1}{6}\begin{bmatrix} 2 & -1 & -1 \\ -1 & -1 & 2 \\ -1 & 2 & -1 \end{bmatrix} \quad T_\beta^{-} = \frac{\sqrt{3}}{6}\begin{bmatrix} 0 & -1 & 1 \\ -1 & 1 & 0 \\ 1 & 0 & -1 \end{bmatrix}$$

When the grid distortion and high-frequency noise are not considered, this scheme can quickly extract the positive and negative sequence components of the imbalance voltage, and can realize instantaneous phase lock with the phase capture scheme proposed later. Therefore, the transient response capability of the grid-tied inverter is improved.

B. ANALYSIS OF FICTIVE ORTHOGONAL VARIABLE BASED ON VIRTUAL FREQUENCY CONSTRUCTION

To reduce the influence of noise on the construction of fictive orthogonal variables, the fictive orthogonal variables is constructed by the trigonometric function, and its expression can be expressed as [21]

$$e_{\mathrm{s}\beta}(k) = e_{\mathrm{s}\perp}(k) = \frac{e_{\mathrm{s}\alpha}(k)\cos(\omega\Delta T) - e_{\mathrm{s}\alpha}(k-1)}{\sin(\omega\Delta T)} \tag{16}$$

The virtual angular frequency $\omega_{\mathrm{n}} = 100\pi\, rad/s$ is constructed with the fundamental angular frequency of the power grid. In the actual power grid, ω is not always equal to ω_{n}, and

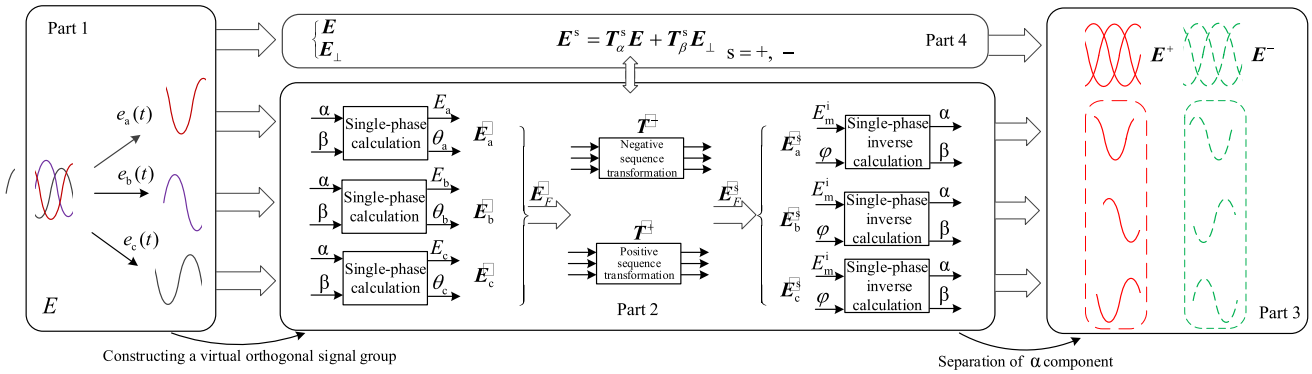

FIGURE 1. Diagram of sequence component measurement.

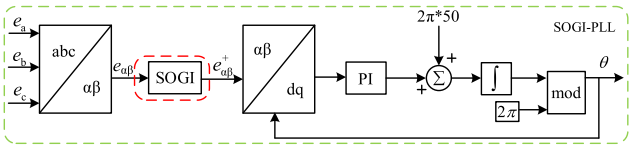

FIGURE 2. Diagram of SOGI-PLL control structure.

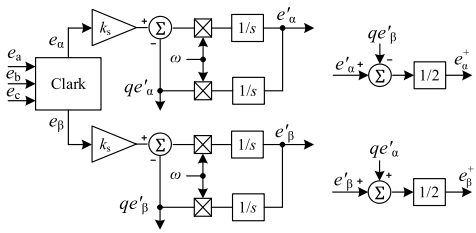

FIGURE 3. Diagram of SOGI structure.

the fictive orthogonal variable will produce corresponding errors. When $\omega \neq \omega_n$, (16) can be rewritten as

$$e'_{s\beta}(k) = \frac{e_{s\alpha}(k)\cos\left[(\omega_n + \Delta\omega)\Delta T\right] - e_{s\alpha}(k-1)}{\sin\left[(\omega_n + \Delta\omega)\Delta T\right]} \tag{17}$$

where $\Delta\omega$ is the frequency deviation.

The virtual angular frequency ω_n replaces ω in formula (16), and the error of the fictive orthogonal variable is deduced as (18), as shown at the bottom of the next page.

It can be seen from (18) that the error of the fictive orthogonal variable mainly comes from $\Delta\omega$ under the virtual angular frequency as the reference. Taking the positive sequence component as an example, substituting (18) into (15), the total error of the sequence component extraction can be deduced as

$$\begin{aligned} E_{rror} &= \boldsymbol{E}^+_{actual} - \boldsymbol{E}^+_{fix} \\ &= \left|\left\{T^+_\alpha \boldsymbol{E} + T^+_\beta \boldsymbol{E}_\perp\right\} - \left\{T^+_\alpha \boldsymbol{E} + \left(1 + \frac{\Delta\omega}{\omega_n}\right) T^+_\beta \boldsymbol{E}_\perp\right\}\right| \\ &= \left|\left(\frac{\Delta\omega}{\omega_n}\right) \times \frac{\sqrt{3}}{6}\begin{bmatrix} 0 & 1 & -1 \\ -1 & 0 & 1 \\ 1 & -1 & 0 \end{bmatrix} \boldsymbol{E}_\perp\right| \\ &\leq \frac{\sqrt{3}}{3}\left(\frac{\Delta\omega}{\omega_n}\right) \boldsymbol{E}_{\max} \end{aligned} \tag{19}$$

When the power system is operating normally, the frequency fluctuation allowed by the power grid is ±0.2Hz [22]. At this time, the error of the fictive orthogonal variable is 0.4%. From (17), it can be seen that the total error of the sequence component is less than the error of the fictive orthogonal variable (0.4%). From this, it can be seen that in applications that do not have strict requirements on accuracy, the extraction of sequence components is sufficient to meet the needs of subsequent control. In the case of large frequency deviation or high accuracy requirements, (16) can be updated through the frequency capture to meet the corresponding accuracy requirements [23], [24].

III. FPC CONTROL OF GRID-TIED INVERTER

A. REAL TIME PHASE CAPTURE METHOD

As shown in Figure 2, the SOGI-PLL needs to design a bandpass filter to extract the positive sequence component of the grid voltage, and track the changing grid voltage through the PI controller, the tacking time of the PLL scheme is about 20ms [5].

Figure 3 shows the structure diagram of SOGI, where the parameter k_s determines the filtering effect of SOGI. When the value of k_s increases, the dynamic response is faster, but the filtering effect will be greatly reduced. The filter effect and response time are considered as a compromise, $k_s = \sqrt{2}$.

In order to shorten the time for the system to withstand negative sequence current and power fluctuations, it is necessary to further improve phase lock speed.

When the grid frequency changes from ω_n to ω, according to (4), positive sequence voltage component can be rewritten as

$$\begin{bmatrix} E_d \\ E_q \end{bmatrix} = \boldsymbol{T}_{abc/dq}(\omega_n t)\begin{bmatrix} e^+_a(t) \\ e^+_b(t) \\ e^+_c(t) \end{bmatrix} \tag{20}$$

Then, the expression of the grid voltage in the SRF can be described as

$$\begin{cases} E_d = E^+_m \cos\left[(\omega - \omega_n)t + \varphi\right] \\ E_q = E^+_m \sin\left[(\omega - \omega_n)t + \varphi\right] \end{cases} \tag{21}$$

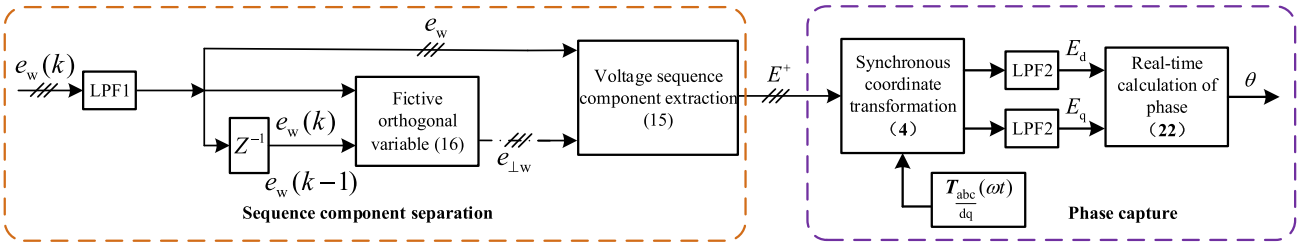

FIGURE 4. Real-time fast phase capture method.

Assumption $\varphi \in [0, 2\pi)$, according to (21), the grid phase can be deduced as

$$\begin{aligned}\theta &= \omega t + \varphi = \omega_n t + (\omega - \omega_n)\, t + \varphi \\ &= \omega_n t + \arctan\left(\frac{E_q}{E_d}\right) + \theta_{extra}\end{aligned} \tag{22}$$

where

$$\theta_{extra} = \begin{cases} 0, & E_d > 0, E_q > 0 \\ \pi, & E_d < 0 \\ 2\pi, & E_d > 0, E_q < 0 \end{cases} \tag{23}$$

Combining (15) and (22) can instantly capture the grid voltage phase. This method is also suitable for capturing the phase of the negative sequence voltage.

B. WAYS TO DEAL WITH NOISE

In the A/D conversion process, the system will inevitably introduce high-frequency random noise. In order to avoid phase lock error caused by high frequency noise. This article introduces a low-pass filter (LPF) to preprocess the voltage signal. Among them, LPF1 filters the original input voltage signal with a cutoff frequency of 10KHz, and LPF2 filters the voltage component under the dq-axis with a cutoff frequency of 5KHz [21].

To sum up, the real-time FPC scheme is shown in Figure 4. Within the normal fluctuation range of the grid frequency, this method can successfully lock phase within 2ms under imbalanced voltage. Compared with the existing PLL scheme, the phase lock speed is significantly increased, thus improving the transient response capability of the inverter.

C. CONTROL SYSTEM

In the SRF, the output power of inverter can be expressed as [18]

$$\begin{aligned} S &= P_e + jQ_e \\ &= (e^{j\omega t}E_{dq}^{+} + e^{-j\omega t}E_{dq}^{-})(e^{j\omega t}I_{dq}^{+} + e^{-j\omega t}I_{dq}^{-})^* \end{aligned} \tag{24}$$

where I is the line current. (24) can be expanded as

$$\begin{cases} P_e = \mathrm{Re}(S) = P_0 + P_S \sin(2\omega t) + P_C \cos(2\omega t) \\ Q_e = Im(S) = Q_0 + Q_S \sin(2\omega t) + Q_C \cos(2\omega t) \end{cases} \tag{25}$$

among them

$$\begin{bmatrix} P_0 \\ P_s \\ P_c \\ Q_0 \\ Q_s \\ Q_c \end{bmatrix} = \frac{3}{2}\begin{bmatrix} E_d^+ & E_q^+ & E_d^- & E_q^- \\ E_q^- & -E_d^- & -E_q^+ & E_d^+ \\ E_d^- & E_q^- & E_d^+ & E_q^+ \\ E_q^+ & -E_d^+ & E_q^- & -E_d^- \\ -E_d^- & -E_q^- & E_d^+ & E_q^+ \\ E_q^- & -E_d^- & E_q^+ & -E_d^+ \end{bmatrix}\begin{bmatrix} I_d^+ \\ I_q^+ \\ I_d^- \\ I_q^- \end{bmatrix} \tag{26}$$

where P_0 and Q_0 are average power components, P_S and P_C, Q_S and Q_C are instantaneous power components.

Combined with the FPC scheme above, the voltage component on the q-axis is 0. For determining the instruction value of current in the current control loop, P_0 and Q_0 are used as the constraint equation.

$$\begin{cases} P_0 = \dfrac{3}{2}\left(E_d^+ I_d^+ + E_d^- I_d^-\right) = P_0^* \\ Q_0 = -\dfrac{3}{2}\left(E_d^+ I_q^+ + E_d^- I_q^-\right) = Q_0^* \end{cases} \tag{27}$$

where: $*$ represents the given value of the corresponding quantity.

Mode I: For controlling the negative sequence current, the given value should be satisfied:

$$I_d^{-*} = I_q^{-*} = 0 \tag{28}$$

According to (28), the current command can be deduced as

$$\begin{bmatrix} I_d^{+*} \\ I_q^{+*} \end{bmatrix} = \frac{2}{3\left(E_d^+\right)^2}\begin{bmatrix} E_d^+ & 0 \\ 0 & -E_d^+ \end{bmatrix}\begin{bmatrix} P_0^* \\ Q_0^* \end{bmatrix} \tag{29}$$

$$\begin{aligned} \lim_{\Delta T \to 0} e_{rror} &= \lim_{\Delta T \to 0} \frac{e_{s\beta}(k)}{e'_{s\beta}(k)} \\ &= \lim_{\Delta T \to 0} \frac{[e_{s\alpha}(k)\cos(\omega_n \Delta T) - e_{s\alpha}(k-1)] \times \sin[(\omega_n + \Delta\omega)\Delta T]}{\sin(\omega_n \Delta T) \times \{e_{s\alpha}(k)\cos[(\omega_n + \Delta\omega)\Delta T] - e_{s\alpha}(k-1)\}} \\ &\approx \frac{(\omega_n + \Delta\omega)}{\omega_n} = 1 + \frac{\Delta\omega}{\omega_n} \end{aligned} \tag{18}$$

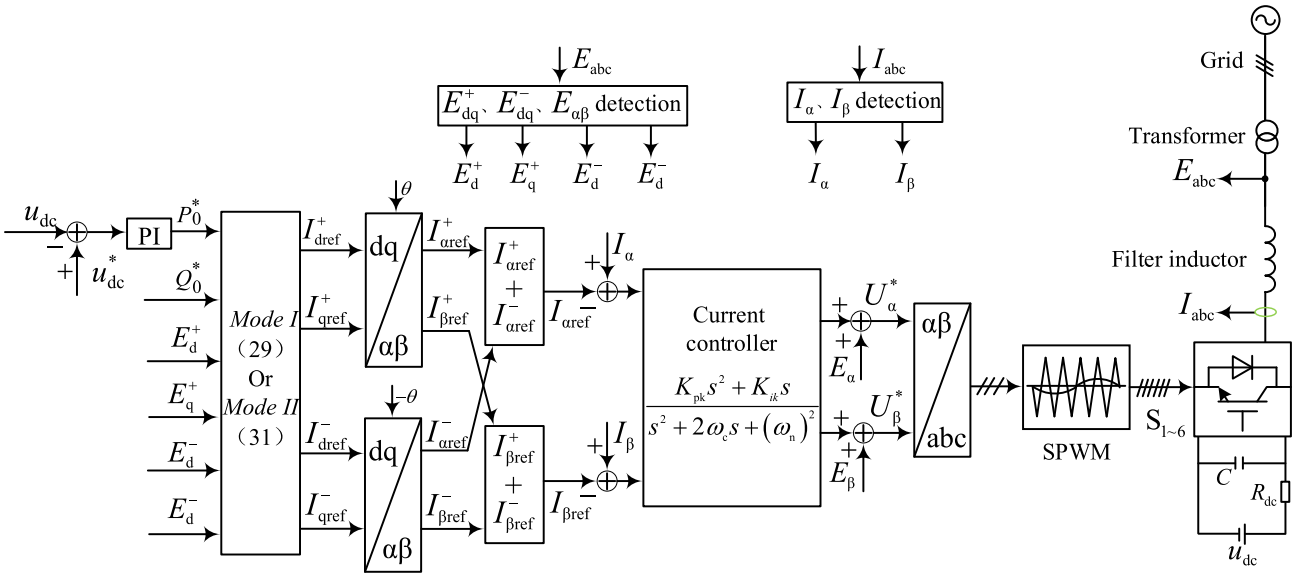

FIGURE 5. Architecture of control system.

Mode II: For suppressing the fluctuation of active power, set $P_s = P_c = 0$ and its expression can be expressed as

$$\begin{cases} P_s = \dfrac{3}{2}\left(E_d^+ I_q^- - E_d^- I_q^+\right) = 0 \\ P_c = \dfrac{3}{2}\left(E_d^- I_d^+ + E_d^+ I_d^-\right) = 0 \end{cases} \tag{30}$$

According to (27), (30), the current command can be defined by

$$\begin{cases} I_d^{+*} = \dfrac{-P_0^* E_d^+}{A}, I_q^{+*} = \dfrac{Q_0^* E_d^+}{B} \\ I_d^{-*} = \dfrac{P_0^* E_d^-}{A}, I_q^{-*} = \dfrac{P_0^* E_d^-}{A} \end{cases} \tag{31}$$

where

$$A = \frac{3}{2}\left(E_d^{-2} - E_d^{+2}\right), \quad B = \frac{3}{2}\left(E_d^{-2} + E_d^{+2}\right)$$

In addition, the equivalent mathematical model of the inverter at SRF can be expressed as [19]

$$\begin{cases} \boldsymbol{U}_{dq}^+ = \boldsymbol{E}_{dq}^+ + \boldsymbol{I}_{dq}^+ R + L\dfrac{d\boldsymbol{I}_{dq}^+}{dt} + j\omega L \boldsymbol{I}_{dq}^+ \\ \boldsymbol{U}_{dq}^- = \boldsymbol{E}_{dq}^- + \boldsymbol{I}_{dq}^- R + L\dfrac{d\boldsymbol{I}_{dq}^-}{dt} - j\omega L \boldsymbol{I}_{dq}^- \end{cases} \tag{32}$$

where $\boldsymbol{U}$ is the inverter output voltage, R and L are the resistance and inductance of the grid side. Through (29), (31), (32), the current command value $\boldsymbol{I}_{dq}^{+*}$, $\boldsymbol{I}_{dq}^{-*}$ under different control targets can be obtained.

In order to avoid independent detection of positive and negative sequence currents, transforming $\boldsymbol{I}_{dq}^{+*}$, $\boldsymbol{I}_{dq}^{-*}$ into the current command value in $\alpha\beta$ frame through coordinate transformation.

$$\boldsymbol{I}_{\alpha\beta}^* = \boldsymbol{I}_{\alpha\beta}^{+*} + \boldsymbol{I}_{\alpha\beta}^{-*} = \boldsymbol{I}_{dq}^{+*} e^{j\omega t} + \boldsymbol{I}_{dq}^{-*} e^{-j\omega t} \tag{33}$$

In this paper, a regulator with a resonance frequency of ω_n is used to form a resonant closed-loop control loop, which provides sufficient control gain for the different control objectives. The regulator transfer function can be expressed [20] as

$$G(s) = \frac{K_{pk} s^2 + K_{ik} s}{s^2 + 2\omega_c s + (\omega_n)^2} \tag{34}$$

where K_{pk} and K_{ik} are the first and second resonance coefficients, and the relationship between them is $K_{ik} = K_{pk} R / L$[20]. ω_c is the bandwidth parameter, and the general value range is 5∼15rad/s.

The average active power [24] can be expressed as

$$P_0^* = \left(K_{vP} + \frac{K_{vI}}{s}\right)\left(u_{dc}^* - u_{dc}\right) \tag{35}$$

where K_{vP} and K_{vI} are voltage regulator proportion and integral gain, respectively.

For obtaining unity power factor operation, $Q_0^* = 0$. According to (34), the reference voltage signal of the inverter can be obtained

$$\boldsymbol{U}_{\alpha\beta}^* = G(s)\left(\boldsymbol{I}_{\alpha\beta}^* - \boldsymbol{I}_{\alpha\beta}\right) + \boldsymbol{E}_{\alpha\beta} \tag{36}$$

According to Figure 5, the current loop control block diagram is shown in Figure 6, where $G_{plant}(s)$ is the transfer function of the inverter main circuit, and $K_{pwm}(s)$ is the PWM small inertia link.

$$G_{plant}(s)\frac{1}{R + sL} \tag{37}$$

When the PWM small inertia link is ignored, the open-loop transfer function of the current loop can be expressed as

$$G_{ol}(s) = \frac{K_{pk} s^2 + K_{ik} s}{s^2 + 2\omega_c s + (\omega_n)^2} \cdot \frac{1}{R + sL} \tag{38}$$

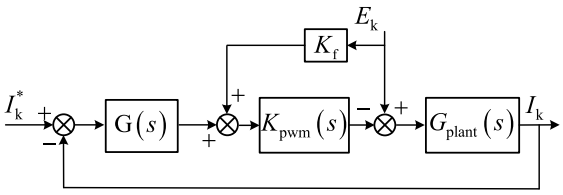

FIGURE 6. Diagram of current loop.

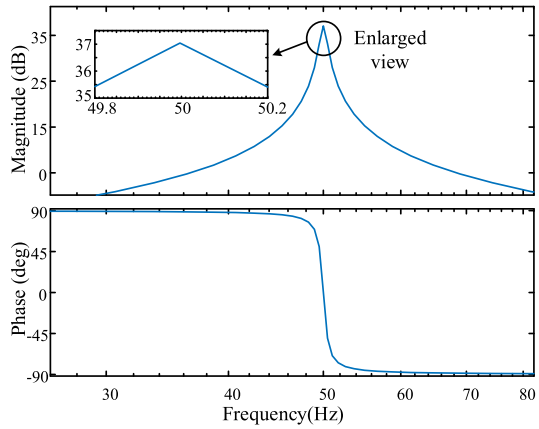

FIGURE 7. Bode diagram of open-loop transfer function.

The Bode diagram of the open-loop transfer function is shown in Figure 7, and its parameters are given in Table 1.

As shown in Figure 7, the amplitude gain of the current controller at the resonant frequency of 50 Hz is 37 dB, indicating that it has a strong ability to adjust at the resonant frequency. When the grid frequency fluctuate is within ±0.2Hz. The lowest resonance gain is 35.5dB, and when the frequency shifts, the controller still has the ability to compensate the negative sequence current or power fluctuation. The open-loop transfer function of the current loop has a phase response of 0° at the resonance frequency, and the maximum phase response near the resonance frequency is around −90°. The closed-loop control response has a phase margin close to 90°. Therefore, the control system is relatively stable.

IV. EXPERIMENTAL VERIFICATIONS

On the RT-LAB experiment platform, the correctness of the FPC control strategy is verified. The architecture of control system and the main parameters are shown in Figure 5 and Table 1. Based on current controller, it is implemented under the SOGI-PLL and FPC control.

In experiment, the control system runs for a period of time under ideal grid voltage conditions, and then changes suddenly (The green line in the experimental graph represents the triggering process of voltage from balanced to imbalanced). The experiment is divided into two parts: suppression of negative sequence current and suppression of active power. The experimental conditions are shown in Table 2.

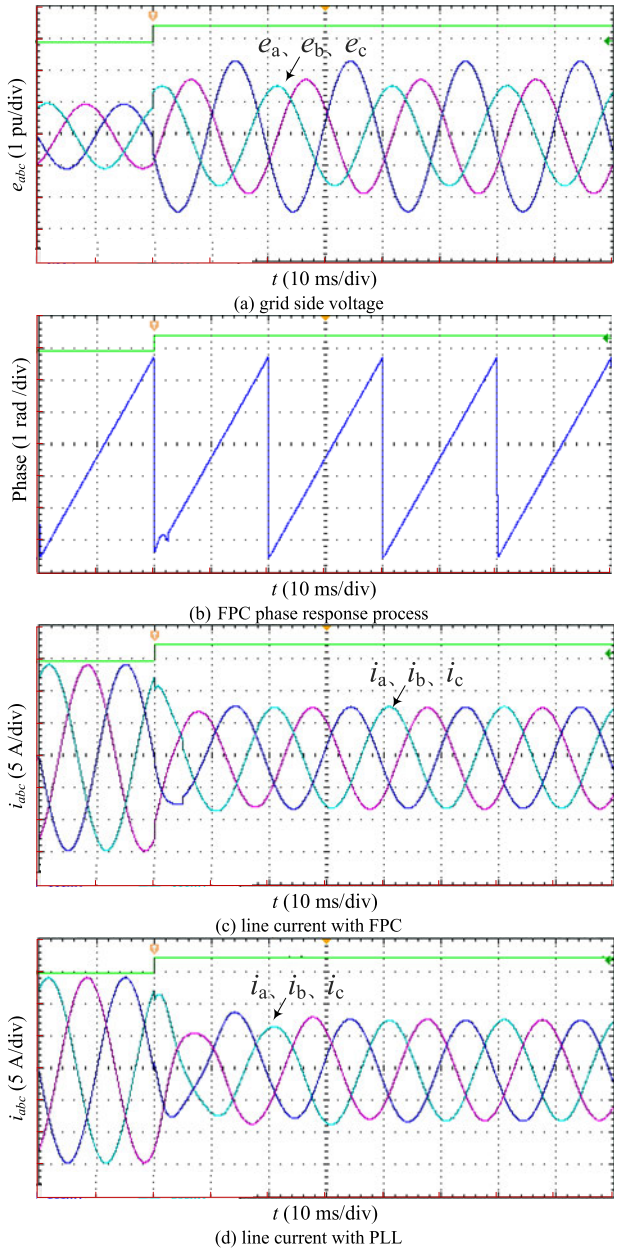

FIGURE 8. Comparison results of negative sequence current compensation.

TABLE 1. Properties parameters of system.

parameter	value	parameter	value
dc side voltage /V	700	Filter inductance /mH	2.4
Sampling frequency /kHz	10	dc side capacitance /mF	3.5
Rated power /kW	7	Filter inductance resistance /Ω	0.1
first resonance coefficients	240	second resonance coefficients	1
PLL proportional parameters	10	PLL integration parameters	100

A. SUPPRESS NEGATIVE SEQUENCE CURRENT AS THE GOAL

When the inverter only operates in *Mode 1*, the current command value should be selected as (29). This experi-

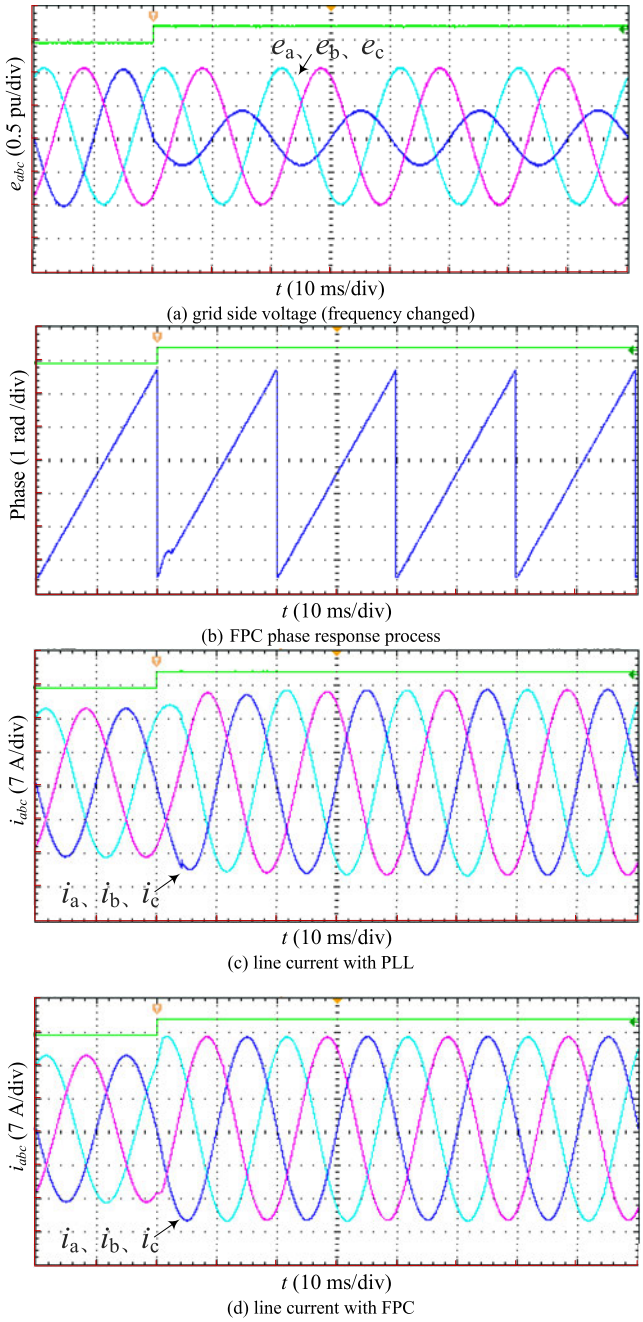

FIGURE 9. Comparison results of negative sequence current compensation (frequency changed).

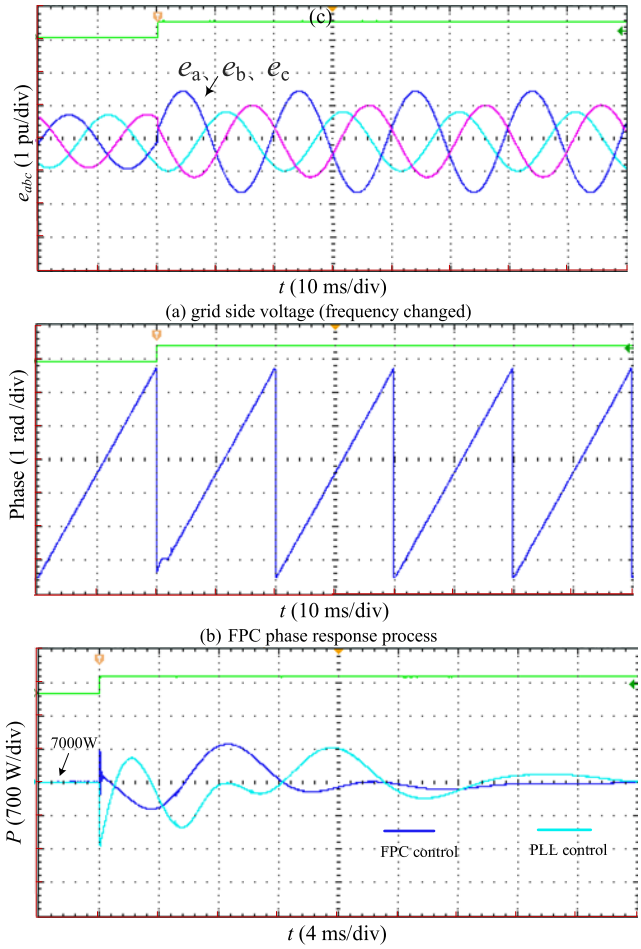

FIGURE 10. Power response process with PLL and FPC (frequency changed).

TABLE 2. Experimental conditions parameters.

conditions	E^+/pu	φ^+/°	E^-/pu	φ^-/°	f/Hz
Normal operation	1.0	0	0	0	50
Suppress negative	1.8	0	0.35	30	50
sequence current	0.8	0	0.4	0	50.2
Suppress active	1.2	0	0.25	45	50.2
power fluctuation	0.6	0	0.45	45	50

TABLE 3. Phase capture time comparison (ms).

Algorithm	Amplitude change	Phase change	Frequency change
DDSRF-PLL	<18	<18	<30
SOGI-PLL	<14	<14	<23
FPC	<2	<2	<2

mental results with SOGI-PLL control and FPC control are shown in Figure 8. Figure 8(a) shows that the grid voltage amplitude and phase have abrupt changes, and the frequency is 50Hz. Figure 8(b) shows the phase response process of the FPC strategy. At this time, the phase capture time mainly depends on the cutoff frequency of the LPF, which is about 2ms.The comparison results of the line current under the two different control strategies are shown in Figure 8(c) and Figure 8(d). It can be concluded that the FPC control strategy compensates the negative sequence current faster.

Figure 9 (a) shows that the single-phase grid voltage drops by 60%. Figure 9 (b) shows the phase capture process of FPC when the grid frequency changes. Within the allowable frequency fluctuation range of the grid, calculating the

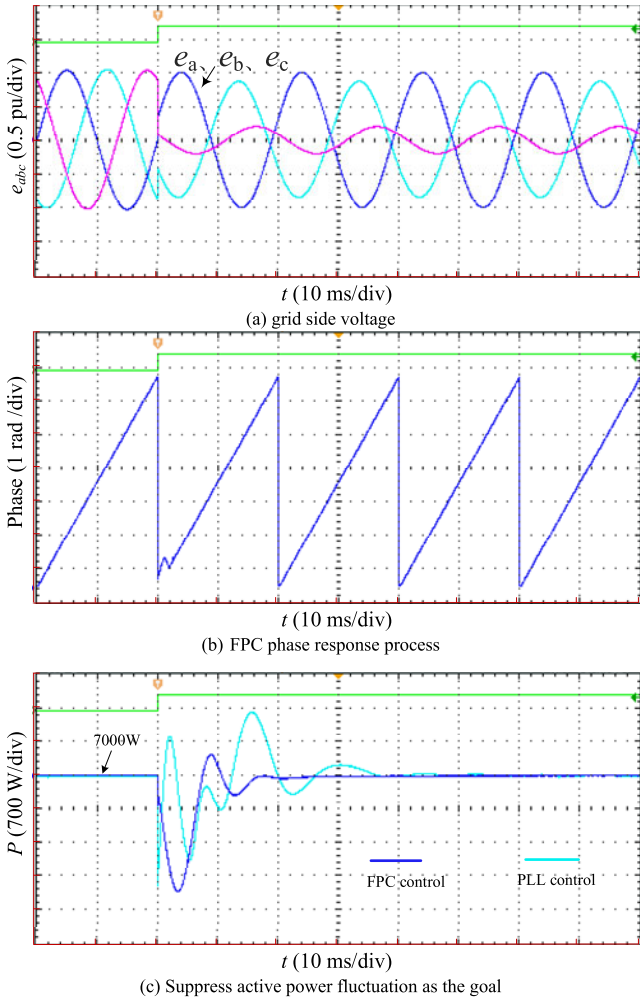

FIGURE 11. Power response process with PLL and FPC.

real-time phase of the grid from the virtual angular frequency can significantly shorten the phase capture process, which is about 2ms. It can be seen from Figure 9 (c), (d), even if the grid frequency changes, the FPC strategy can still quickly compensate for the negative sequence current.

B. SUPPRESS ACTIVE POWER FLUCTUATION AS THE GOAL

Figure 10 (a) shows that the grid voltage suddenly changes in amplitude, phase and frequency. Figure 10 (b) shows the acquisition process of the grid voltage phase when the frequency changes, which is about 2ms. Figure 10 (c) shows the power response process, the power response time of the FPC control is faster, about 15ms.

Figure 11 (a) shows a severe drop in single-phase voltage. Figure 11 (b) shows the phase capture process of the grid voltage, which is about 2ms. Figure 11 (c) shows the active power response process under the two strategies. Compared with the power response under SOGI-PLL control, the FPC power response is faster, about 16ms.

Table 3 shows the dynamic response time comparison between different PLL schemes and the FPC scheme in phase capture. FPC has obvious advantages in-phase response, so the inverter maintains good control performance during the transient response.

V. CONCLUSION

Compared with traditional methods, the main advantages of the proposed FPC control strategy are summarized as follows:

1) The FPC strategy does not need to adjust PLL parameters and simplifies the control structure of the system.

2) Within the frequency fluctuation range allowed by the power grid, compared with previous PLL schemes, FPC strategy has significant advantages in phase capture speed. which enhances the fault ride-through capability of the inverter.

3) The FPC strategy does not need to separate sequence current components, avoids feedforward decoupling control, and further simplifies the structure of the controller.

Follow-up will further expand the application of FPC in harmonic control such as APF.

REFERENCES

[1] L. Xiong, X. Liu, C. Zhao, and F. Zhuo, "A fast and robust real-time detection algorithm of decaying DC transient and harmonic components in three-phase systems," *IEEE Trans. Power Electron.*, vol. 35, no. 4, pp. 3332–3336, Apr. 2020.

[2] W. Binbing, X. Abuduwayiti, C. Yuxi, and T. Yizhi, "RoCoF droop control of PMSG-based wind turbines for system inertia response rapidly," *IEEE Access*, vol. 8, pp. 181154–181162, 2020, doi: 10.1109/ACCESS.2020.3027740.

[3] T. Xia, X. Zhang, G. Tan, and Y. Liu, "Synchronous reference frame single-phase phase-locked loop (PLL) algorithm based on half-cycle DFT," *IET Power Electron.*, vol. 13, no. 9, pp. 1893–1900, Jul. 2020.

[4] D. Venkatramanan and V. John, "Dynamic phasor modeling and stability analysis of SRF-PLL-based grid-tie inverter under islanded conditions," *IEEE Trans. Ind. Appl.*, vol. 56, no. 2, pp. 1953–1965, Mar./Apr. 2020.

[5] M. Xie, H. Wen, C. Zhu, and Y. Yang, "DC offset rejection improvement in single-phase SOGI-PLL algorithms: Methods review and experimental evaluation," *IEEE Access*, vol. 5, pp. 12810–12819, 2017.

[6] S. Golestan, S. Y. Mousazadeh, J. M. Guerrero, and J. C. Vasquez, "A critical examination of frequency-fixed second-order generalized integrator-based phase-locked loops," *IEEE Trans. Power Electron.*, vol. 32, no. 9, pp. 6666–6672, Sep. 2017.

[7] L. Du, M. Li, Z. Tang, L. Xiong, X. Ma, and G. Tang, "A fast positive sequence components extraction method with noise immunity in unbalanced grids," *IEEE Trans. Power Electron.*, vol. 35, no. 7, pp. 6682–6685, Jul. 2020.

[8] D. Zhu, S. Zhou, X. Zou, and Y. Kang, "Improved design of PLL controller for LCL-type grid-connected converter in weak grid," *IEEE Trans. Power Electron.*, vol. 35, no. 5, pp. 4715–4727, May 2020.

[9] S. Golestan, F. D. Freijedo, A. Vidal, A. G. Yepes, J. M. Guerrero, and J. Doval-Gandoy, "An efficient implementation of generalized delayed signal cancellation PLL," *IEEE Trans. Power Electron.*, vol. 31, no. 2, pp. 1085–1094, Feb. 2016.

[10] S. Golestan, M. Ramezani, J. M. Guerrero, and M. Monfared, "Dq-frame cascaded delayed signal Cancellation-based PLL: Analysis, design, and comparison with moving average filter-based PLL," *IEEE Trans. Power Electron.*, vol. 30, no. 3, pp. 1618–1632, Mar. 2015.

[11] R. H. Yang, B. A. McDonald, and Y. Li, "Investigation on the small signal characteristic based on the LLC hybrid hysteretic charge control," *CPSS Trans. Power Electron. Appl.*, vol. 4, no. 2, pp. 128–142, Jun. 2019.

[12] L. Xiong, F. Zhuo, X. Liu, Z. Xu, and Y. Zhu, "Fault-tolerant control of CPS-PWM-based cascaded multilevel inverter with faulty units," *IEEE J. Emerg. Sel. Topics Power Electron.*, vol. 7, no. 4, pp. 2486–2497, Dec. 2019.

[13] H. Nian, Y. Shen, H. Yang, and Y. Quan, "Flexible grid connection technique of voltage-source inverter under unbalanced grid conditions based on direct power control," *IEEE Trans. Ind. Appl.*, vol. 51, no. 5, pp. 4041–4050, Sep. 2015.

[14] M. Brenna, F. Foiadelli, and D. Zaninelli, "New stability analysis for tuning PI controller of power converters in railway application," *IEEE Trans. Ind. Electron.*, vol. 58, no. 2, pp. 533–543, Feb. 2011.
[15] C. Zou, B. Liu, S. Duan, and R. Li, "Stationary frame equivalent model of proportional-integral controller in dq synchronous frame," *IEEE Trans. Power Electron.*, vol. 29, no. 9, pp. 4461–4465, Sep. 2014.
[16] S. Gulur, V. M. Iyer, and S. Bhattacharya, "A dual-loop current control structure with improved disturbance rejection for grid-connected converters," *IEEE Trans. Power Electron.*, vol. 34, no. 10, pp. 10233–10244, Oct. 2019.
[17] D. Yang, N. Wu, L. Yin, and Z. Lu, "Natural frame control of single-phase cascaded H-bridge multilevel converter based on fictive-phases construction," *IEEE Trans. Ind. Electron.*, vol. 65, no. 5, pp. 3848–3857, May 2018.
[18] H. Nian and L. Li, "Direct power control of doubly fed induction generator without phase-locked loop under harmonically distorted voltage conditions," *IEEE Trans. Power Electron.*, vol. 33, no. 7, pp. 5836–5846, Jul. 2018.
[19] L. Li, H. Nian, L. Ding, and B. Zhou, "Direct power control of DFIG system without phase-locked loop under unbalanced and harmonically distorted voltage," *IEEE Trans. Energy Convers.*, vol. 33, no. 1, pp. 395–405, Mar. 2018.
[20] D. Zhu, S. Zhou, X. Zou, Y. Kang, and K. Zou, "Small-signal disturbance compensation control for LCL-type grid-connected converter in weak grid," *IEEE Trans. Ind. Appl.*, vol. 56, no. 3, pp. 2852–2861, May 2020.
[21] L. Xiong, F. Zhuo, F. Wang, X. Liu, and M. Zhu, "A fast orthogonal signal-generation algorithm characterized by noise immunity and high accuracy for single-phase grid," *IEEE Trans. Power Electron.*, vol. 31, no. 3, pp. 1847–1851, Mar. 2016.
[22] *Power Quality-Frequency Deviation for Power System*, document GB/T15945, 2008.
[23] K.-J. Lee, J.-P. Lee, D. Shin, D.-W. Yoo, and H.-J. Kim, "A novel grid synchronization PLL method based on adaptive low-pass notch filter for grid-connected PCS," *IEEE Trans. Ind. Electron.*, vol. 61, no. 1, pp. 292–301, Jan. 2014.
[24] T. Wen, D. Zhu, X. Zou, B. Jiang, L. Peng, and Y. Kang, "Power coupling mechanism analysis and improved decoupling control for virtual synchronous generator," *IEEE Trans. Power Electron.*, vol. 36, no. 3, pp. 3028–3041, Mar. 2021, doi: 10.1109/TPEL.2020.3017254.

WU BINBING was born in Sichuan, China. He received the B.S. degree from the Shenyang University of Technology, Shenyang, China, in 2017. He is currently pursuing the master's degree with Xinjiang University, China.

His current research interests include power electronics and renewable power generation.

TIAN YIZHI was born in Urumqi, Xinjiang, China, in 1983. He received the B.S. degree from NCEPU, China, in 2006, and the M.S. and Ph.D. degrees from the College of Electrical Engineering, Xinjiang University, China, in 2010 and 2015, respectively.

He was an Assistant Professor with the College of Electrical Engineering, Xinjiang University. He is the author of five articles and six inventions. His research interests include renewable energy stability and integrated energy systems.

CHEN YUXI was born in Yangzhou, China. She received the B.S. degree from the Nanjing Institute of Technology, Nanjing, China, in 2020. She is currently pursuing the master's degree with The University of Sheffield, U.K.

Her current research interests include automatic control and systems engineering.

XIWANG ABUDUWAYITI was born in Urumqi, China. He received the B.S. degree from the Dalian University of Technology, Dalian, China, in 1995.

He is currently an Associate Professor with Xinjiang University, China. His current research interest includes power quality management.

LIANSONG XIONG (Member, IEEE) was born in Guangyuan, Sichuan, China, in 1986. He received the B.S., M.S., and Ph.D. degrees in electrical engineering from Xi'an Jiaotong University (XJTU), Xi'an, China, in 2009, 2012, and 2016, respectively. Since 2014, he has been with the School of E-Learning, XJTU, as a Part-Time Faculty Member. In 2016, he joined the School of Automation, Nanjing Institute of Technology (NJIT), Nanjing, China, introduced in High-Level Academic Talent Plan of NJIT. From 2017 to 2019, he was with the Department of Electrical Engineering, The Hong Kong Polytechnic University (Poly U), Hong Kong, as a Research Associate. He is the first author of nine articles indexed by SCI and more than 20 articles indexed by EI. His current research interests include power quality, multilevel converter, renewable energy generation, and stability analysis of converter-dominated power systems. He is a Senior Member of the China Electrotechnical Society and a member of the China Power Supply Society and the China Society for Electrical Engineering. He received the Excellent Paper Award seven times in academic conferences and the National Scholarship for the Graduate Students in three consecutive years.